High Curie-temperature ferromagnetism in cobalt-implanted single-crystalline rutile

2004 J. Phys.: Condens. Matter 16 L443

(http://iopscience.iop.org/0953-8984/16/41/L03)

INSTITUTE OF PHYSICS PUBLISHING JOURNAL OF PHYSICS: CONDENSED MATTER

J. Phys.: Condens. Matter **16** (2004) L443–L449 PII: S0953-8984(04)83093-5

LETTER TO THE EDITOR

High Curie-temperature ferromagnetism in cobalt-implanted single-crystalline rutile

R I Khaibullin[1,2], L R Tagirov[2,3,4], B Z Rameev[1,2], Sh Z Ibragimov[3], F Yıldız[2] and B Aktaş[2]

[1] Kazan Physical-Technical Institute of RAS, Sibirsky Trakt 1017, 420029 Kazan, Russia
[2] Gebze Institute of Technology, P. K. 141, 41400 Gebze-Kocaeli, Turkey
[3] Kazan State University, Kremlevskaya str. 18, 420008 Kazan, Russia

E-mail: Lenar.Tagirov@ksu.ru

Received 28 June 2004, in final form 2 August 2004
Published 1 October 2004
Online at stacks.iop.org/JPhysCM/16/L443
doi:10.1088/0953-8984/16/41/L03

Abstract

The ion implantation technique has been used to fabricate a Co-rich layer in rutile: single-crystalline TiO_2 substrates were heavily irradiated by Co^+ ions with energy of 40 keV. The magnetic properties of as-prepared and post-annealed samples were studied by both inductive and Faraday magnetometry as well as ferromagnetic resonance (FMR). A ferromagnetic Curie temperature as high as 700 K was measured in our samples. The analysis of the magnetic hysteresis loop, the temperature dependence of the saturation magnetization, and strong out-of-plane anisotropy of the FMR spectra allow us to suppose that the origin of the macroscopic high-temperature ferromagnetism is the exchange interaction mediated by oxygen vacancies.

1. Introduction

It has been shown recently that new functionality can be implemented by the injection, transport and control of the carriers' spin-polarization in semiconductors (see, for example, reviews [1–4]). However, the injection of a spin-polarized current from conventional ferromagnetic metals, like iron or nickel, into a semiconducting structure encounters serious problems because of the large mismatch in conductivities and other band properties between the metal and the semiconductor. One possible solution is a semiconducting spin-polarized injector. Moreover, magnetic semiconductors have the advantage that they can be easily combined with conventional semiconductor circuits. Since the work by Matsumoto *et al* [5], the magnetically doped wide-band semiconductor $Co_xTi_{1-x}O_2$, prepared by laser molecular beam epitaxy, has been proposed as a room-temperature injector of spin-polarized current into semiconducting

[4] Author to whom any correspondence should be addressed.

structures [6–8]. Subsequently, ferromagnetic cobalt-doped TiO_2 films of rutile structure have been deposited by reactive co-sputtering [9] and investigated by Moodera *et al* [10, 11].

Recently, the ion implantation technique has been employed for the magnetic doping of titanium dioxide of anatase structure, and super-paramagnetic cobalt nanoclusters have been formed in a TiO_2 host [12]. In [13], room temperature ferromagnetism was observed in rutile TiO_2 (110) implanted with Co ions at a very high temperature of the substrate (1075 K). However, the actual Curie temperature was not reported, and the value of the remanent magnetization at room temperature was a small fraction of the saturation magnetization. In this letter we report on the results of high-dose implantation with cobalt ions into rutile-structure TiO_2 substrates kept at room temperature. The as-implanted samples show high Curie-temperature ferromagnetism ($\sim$750 K) with the magnetic properties corresponding to the bulk ferromagnetic media. Analysis of our magnetic and FMR measurements supposes that oxygen vacancies induced by the ion irradiation strongly support the high-temperature ferromagnetism in the Co-implanted rutile. The observed ferromagnetism is stable during a year of storage at ambient conditions; this is an important issue for possible spintronic applications.

2. Sample preparation and experimental techniques

The 10×10 mm^2 single-crystalline rutile plates (*MTI Corp.*) were implanted with 40 keV Co^+ ions to a dose of 2×10^{17} ions cm^{-2} at an ion current density of 8–9 μA cm^{-2}. The sample holder was cooled by flowing water during the implantations to prevent the samples from overheating. The (100)- and (001)-face rutile plates were irradiated in a single run of an *ILU-3* ion accelerator. Then, the implanted substrates were cut by a diamond cutter into smaller pieces for the subsequent heat treatment and for the structural, magnetic and electrical studies. Various sets of implanted rutile samples were prepared by annealing for 1 h either in a medium vacuum (a residual pressure $\sim 10^{-6}$ Torr), or in air and oxygen (ambient pressure) at temperature $T_{\rm ann} = 950\,^{\circ}$C. The elemental composition and crystalline structure of the surface layers of both as-implanted and subsequently annealed samples were analysed on a Philips XL-30ESEM scanning electron microscope, on an EMR-100 electron diffraction microscope, and on a Rigaku RINT 2000 series x-ray diffractometer. The magnetic properties of the implanted rutile samples were investigated by inductive magnetometry, Faraday magnetometry and the magnetic resonance technique. A home-made rotating sample magnetometer [14] was used to record the magnetic hysteresis loop at room temperature. The temperature dependence of the saturation magnetization in the temperature range 100–1000 K was measured by the Faraday balance technique [15]. The magnetic resonance spectra were recorded on a Bruker EMX electron spin resonance (ESR) spectrometer at x-band frequency (9.8 GHz) in the temperature range 10–300 K and for various orientations of the sample with respect to the applied DC magnetic field H. The field derivative of the microwave power absorption, $\mathrm{d}P/\mathrm{d}H$, was registered as a function of the field H.

3. Magnetometry and ferromagnetic resonance measurements of as-implanted samples

Figure 1 shows the results of magnetization measurements in two orientations of the external field relative to the sample plane. The magnetic hysteresis loop in the in-plane scan geometry of the measurement clearly demonstrates ferromagnetism of the Co-implanted layer at room temperature. The net ferromagnetic moment per implanted Co ion was estimated from the saturation magnetization at room temperature as $\sim 0.4 \pm 0.05 \mu_{\rm B}$ for the (100) samples and $\sim 0.55 \pm 0.05 \mu_{\rm B}$ for the (001) samples. The coercive field is $H_{\rm c} \simeq 195$ Oe for (100)-TiO_2

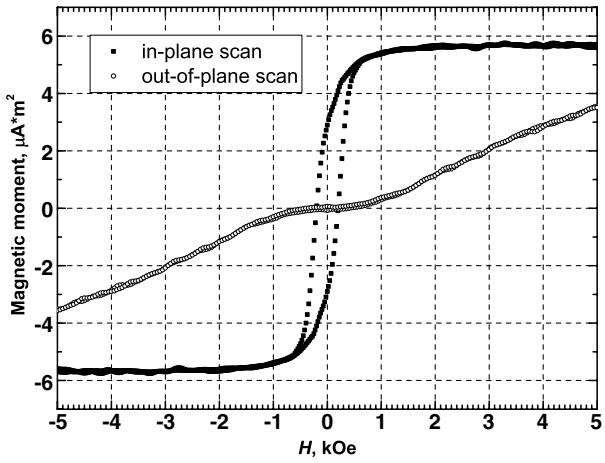

Figure 1. The magnetization measurements on the as-prepared (100) sample at room temperature.

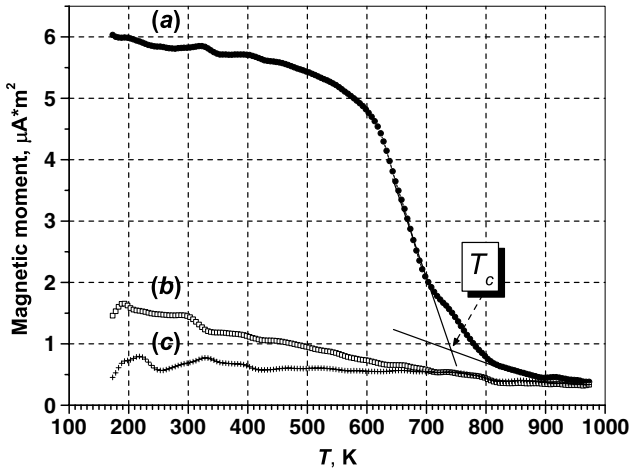

Figure 2. The dependence of the saturation magnetization on temperature for the (100) sample measured at 2 kOe. (a): first heating-cooling cycle; (b): repeated cycle; (c): after annealing in air.

and $\simeq$65 Oe for (001)-TiO_2; the remanence to saturation ratio is $M_{\rm rem}/M_{\rm sat} \sim 0.5$–$0.6$. It is worth mentioning that the in-plane remanent magnetization did not decrease over several days. There is small but detectable remanent magnetization in the field direction perpendicular to the sample surface (out-of-plane scan).

Figure 2(a) displays the temperature dependence of the saturation magnetization for the (100) sample with Curie temperature $T_{\rm c}(100) \simeq 750$ K ($T_{\rm c}(001) \simeq 720$ K). The thermo-magnetic curve shows bulk-like behaviour of magnetization, with a high-temperature tail persisting up to 1000 K. Repeated measurements revealed a considerable decrease of the saturation magnetization—about 3–4 times in the low-temperature region—after the first thermo-cycle (figure 2(b)). Simultaneously, the overall curvature of the thermo-magnetic curve became negative (a concave shape as opposed to the first-heating mixed shape curve).

The upper and lower panels of figure 3 represent the magnetic resonance spectra recorded from the as-implanted samples for two orientations, $\theta = 0^\circ$ and 90°, of the applied magnetic

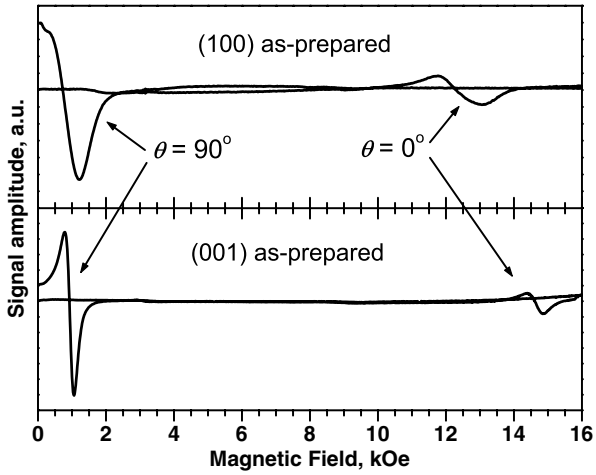

Figure 3. FMR spectra recorded at two orientations of DC magnetic field with respect to the sample normal.

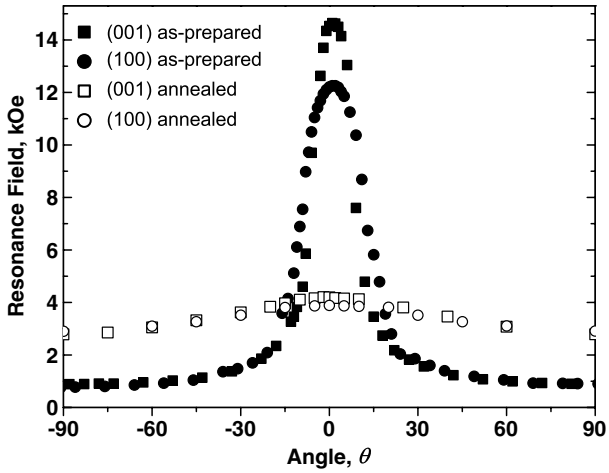

Figure 4. The angular dependence of the out-of-plane FMR fields for resonance: solid symbols, as-implanted samples; open symbols, after annealing in vacuum.

field relative to the normal to the implanted surface, respectively. Figure 4 displays the full out-of-plane angular dependence of the resonance field against the polar angle θ (solid symbols). The resonance shows very strong anisotropy which resembles qualitatively the behaviour of an FMR signal for thin continuous ferromagnetic films [16, 17]. For ferromagnets, the resonance field depends on the orientation of the film plane with respect to the magnetic field because of the macroscopic demagnetization field. Guided by the observation of the ferromagnetic film-like anisotropy of the FMR signal we applied the Kittel set of equations [18] for the two orientations of the magnetic field with respect to the normal direction to the plane of the sample to determine the effective magnetization M_{eff}:

$$h\nu_0 = g\mu_{\text{B}}(H_{\perp} - 4\pi M_{\text{eff}}), \tag{1}$$

$$h\nu_0 = g\mu_{\text{B}}\sqrt{H_{\parallel}(H_{\parallel} + 4\pi M_{\text{eff}})}, \tag{2}$$

where equation (1) corresponds to $\theta = 0°$ and equation (2) to $\theta = 90°$. ν_0 and $H_{\parallel}(H_{\perp})$ are the experimental values of the microwave frequency and resonance magnetic field, respectively, g is the spectroscopic g-factor and μ_B is the Bohr magneton. Using the experimental data for the resonance field at $\theta = 0°$ ($H_{\perp}$) and $\theta = 90°$ ($H_{\parallel}$) from figure 4 (solid symbols) we determined the effective saturation magnetization: $M_{\rm eff}(100) \simeq 735$ G and $M_{\rm eff}(001) \simeq 900$ G. It is worth mentioning that the FMR studies were repeated on the same samples after one year of exposition to a humid atmosphere, but we could not notice any change in the intensity or shape of the resonance lines.

4. Influence of heat treatment on the magnetic properties

Considerable weakening of the FMR response was observed in the vacuum-annealed samples. Figure 4, open symbols, shows the out-of-plane angular dependence of the FMR field for resonance. Using equations (1) and (2) we determined the effective saturation magnetization: $M_{\rm eff}$(100-annealed) $\simeq 53$ G and $M_{\rm eff}$(001-annealed) $\simeq 77$ G. The ferromagnetism disappears completely in the samples annealed in air or oxygen (see curve (c) in figure 2). However, a highly anisotropic ESR signal with a hyperfine splitting typical for paramagnetic Co ions [19] was observed at temperatures below 30 K. This fact, as well as the brightening and colouration of the samples after air/oxygen annealing (light red-orange in (001) and light green in (100) samples), reveals that Co^{2+} ions have occupied crystallographic positions in the rutile lattice. A detailed analysis of the ESR spectra will be given elsewhere.

5. Discussion

According to the *SRIM-2003* code [20], the mean projected range is ∼23 nm and the straggling is about 9 nm in the Gaussian depth profile for 40 keV Co^+ ions in rutile. As a result, a buried layer saturated by the Co dopant is formed in the implanted region of TiO_2. Because of the small thickness of the Co-rich layer and the low solubility of the Co dopant in rutile, at implantation doses of about 10^{16} ions cm^{-2} the concentration of the Co dopant already oversaturates, and metallic nanoclusters may grow, as was observed in Co-implanted anatase [12]. However, the possibility of formation of nanoparticles, as well as their size and shape, depends strongly on the implantation regime, the crystal structure of the substrate and on subsequent thermal annealing. Note that another important motivation for the post-implantation heat treatment is annealing of the radiation defects and the recovery of crystallinity of the irradiated substrate. The surface layer of about 10 nm thickness plays the role of effective protection of the synthesized metallic nanoparticles against oxidation in ambient atmosphere.

The observation of a hysteresis loop and strong out-of-plane anisotropy of the FMR signal in the as-implanted samples is consistent with formation of a thin layer of metallic cobalt particles according to the scenario described above. Following the approach developed in [21–23], we may treat the FMR signal as coming from the thin magnetic film with an effective magnetization, which is the bulk saturation magnetization M_s of Co reduced by a volume filling factor η: $M_{\rm eff} = M_s\eta$. Using the bulk value for the saturation magnetization of Co at room temperature [24], M_s(Co) $= 1416$ G, we deduce roughly the filling factor $\eta \sim 0.5$–0.6. Thus, we may derive the conclusion that the FMR signal comes from a dense granular film. The observed out-of-plane anisotropy of the FMR spectra indicates the appearance of a macroscopic demagnetization field, which originates from dipole–dipole interaction between particles and their magnetic percolation into a continuous layer. Thus, our magnetic resonance measurements let us suggest the formation of a metallic cobalt granular

film beneath the surface layer of the as-implanted rutile substrates. However, contrary to the above analysis of the FMR data, we failed to detect any signal from metallic cobalt in our XRD measurements of the samples, either in normal incidence or in grazing incidence. Only traces of oxide Co_3O_4 or spinel phase, Co_2TiO_4, have been observed. These Co-based oxides are antiferromagnets or ferrimagnets with low Néel temperatures. Another suspicious detail is the FMR signal linewidth. One would expect much broader resonance lines if the film is granular with wide distribution of the particle size and interparticle distance (compare the spectra from figure 3 with those in [11]).

An alternative possibility to explain the strong ferromagnetism in Co-implanted TiO_2 rutile is the model proposed recently by Coey *et al* [25] to explain room temperature ferromagnetism in the Fe-doped SnO_2 system. They hypothesized that trivalent iron atoms in their system are coupled via electrons trapped by charge-compensating oxygen vacancies. Because of the high dielectric permittivity of SnO_2 (the refraction index is about 2.1) a large-radius trapping centre is formed at the oxygen vacancy site. This extended electron state effectively couples neighbouring iron ions, forming a homogeneous ferromagnetic state in the dilute Fe:SnO_2 system.

Let us try to look at our data from the viewpoint of the F-centre exchange model. According to the *SRIM-2003* simulation, every incident Co^+ ion generates one titanium and four oxygen vacancies. Most of the implanted cobalt ions may occupy host titanium vacancies and should be in Co^{2+} or Co^{3+} valence states. Stability of the system is provided by the charge-compensating oxygen vacancies. The high refraction index (2.6–2.9) and permittivity of rutile, which means more extended electron orbitals at trapping centres, provide a long range of exchange interaction which couples the local spins of Co ions into the ferromagnetic state.

The mean-field shape of the thermo-magnetic curve (a) in figure 2 indicates the bulky character of the ferromagnetic order below $\sim$700 K, with the majority of Co dopant involved in the macroscopic order. The high-temperature tail may be attributed to super-paramagnetic nanoparticles of metallic cobalt which accumulate an essential minority of the implant and are beyond the sensitivity of our XRD. One may expect that annealing of the oxygen vacancies—mediators of the exchange coupling between Co ions—will weaken or destroy the macroscopic ferromagnetism. In fact, the decrease of the saturation magnetization after the first thermal cycle (see curve (b) in figure 2) can be explained by annealing of the oxygen vacancies during the measurement cycle. The remaining magnetization can be attributed to the assembly of isolated Co nanoparticles. This may be identified from the disappearance of the mean-field part of the temperature dependence of the magnetization and the change of the curve shape to a concave type, typical for assemblies of non-interacting Co nanoparticles (see figure 4 in [10], figure 2 in [12], and figure 6 in [26]). The long-time annealing of the samples in air or oxygen gives rise to complete curing of the oxygen vacancies, oxidation of the larger Co nanoparticles, and the formation of the spinel phases. The FMR data are also consistent with the above picture: the FMR signal from the as-prepared samples (see figure 3) is too narrow to be attributed to the non-interacting Co nanoparticles of various shapes (compare with figures 1 and 2 of [11]). After annealing of the as-implanted samples in vacuum the effective magnetization determined from FMR decreases more than ten times (see figure 4), but the linewidth increases 3–5 times, which correlates with a transition from bulk molecular-field-type ferromagnetism to granular-type ferromagnetism.

Thus, we are inclined to conclude that our experimental data can be consistently explained by the mechanism of exchange between Co ions via the charge-compensating oxygen vacancies produced upon ion implantation. The failure of observation of high Curie-temperature ferromagnetism in other experiments [5–10, 12] may be due to the low concentration of oxygen vacancies in the samples fabricated by other techniques (molecular beam epitaxy, co-sputtering,

sol–gel). We believe that the high dielectric permittivity of the host oxide semiconductor and the ion implantation technique, which provides a high concentration of oxygen vacancies, are the necessary conditions for the synthesis of a conducting ferromagnetic oxide with high Curie temperature. It is an important issue that the ion implantation technique allows the resistivity of the samples to be varied over a wide range by varying the implantation dose or co-doping with non-magnetic ions. We are going to perform a course of investigations to verify the oxygen-vacancy-mediated ferromagnetism in doped oxides.

The work was supported by the RAS Programme 'Low-dimensional quantum structures' and RFBR grant No 03-05-64895. RIK gratefully acknowledges the support of a NATO/TUBITAK Advanced Fellowship Programme, LRT acknowledges support by BRHE through grant REC-007.

References

[1] Ohno H 1999 *J. Magn. Magn. Mater.* **200** 110
[2] Wolf S A, Awschalom D D, Buhrman R A, Daughton J M, von Molnar S, Roukes M L, Chtchelkanova A Y and Treger D M 2001 *Science* **294** 1488
[3] Ohno H, Matsukura F and Ohno F 2002 *JSAP Int.* (5) 4
[4] Matsukura F, Ohno H and Dietl T 2002 III–V ferromagnetic semiconductors *Handbook of Magnetic Materials* vol 1, ed K H J Buschow (Amsterdam: Elsevier) p 1
[5] Matsumoto Y, Murakami M, Shono T, Hasegawa T, Fukumura T, Kawasaki M, Ahmet P, Chikyow T, Koshihara S and Koinuma H 2001 *Science* **291** 854
[6] Soo Y L, Kioseoglou G, Kim S, Kao Y H, Devi P S, Parise J, Gambino R J and Gouma P I 2002 *Appl. Phys. Lett.* **81** 655
[7] Kim D H, Yang J S, Lee K W, Bu S D, Noha T W, Oh S-J, Kim Y-W, Chung J-S, Tanaka H, Lee H Y and Kawai T 2002 *Appl. Phys. Lett.* **81** 2421
[8] Stampe P A, Kennedy R J, Xin Y and Parker J S 2003 *J. Appl. Phys.* **93** 7864
[9] Park W K, Ortega-Hertogs R J, Moodera J, Punnoose A and Seehra M S 2002 *J. Appl. Phys.* **91** 8093
[10] Punnoose A, Seehra M S, Park W K and Moodera J S 2003 *J. Appl. Phys.* **93** 7867
[11] Rameev B Z, Yıldız F, Tagirov L R, Aktaş B, Park W K and Moodera J S 2003 *J. Magn. Magn. Mater.* **258/259** 361
[12] Kim D H, Yang J S, Kim Y S, Kim D-W, Noh T W, Bu S D, Kim Y-W, Park Y D, Pearton S J, Jo Y and Park J-G 2003 *Appl. Phys. Lett.* **83** 4574
[13] Shutthanandan V, Thevuthasan S, Heald S M, Droubay T, Engelhard M H, Kaspar T C, McCready D E, Saraf L, Chambers S A, Mun B S, Hamdan N, Nachimuthu P, Taylor B, Sears R P and Sincovic B 2004 *Appl. Phys. Lett.* **84** 4466
[14] Iasonov P G, Nourgaliev D K, Bourov B V and Heller F 1998 *Geol. Carpathica* **49** 224
[15] Bourov B, Iasonov P, Nourgaliev D and Ibragimov Sh 1996 *Ann. Geophys.* **14** (Suppl. 1) 133
[16] Heinrich B and Cochran J F 1993 *Adv. Phys.* **42** 523
[17] Farle M 1998 *Rep. Prog. Phys.* **61** 755
[18] Kittel C 1978 *Introduction to Solid State Physics* 4th edn (New York: Wiley) p 618
[19] Yamaka E and Barnes R G 1962 *Phys. Rev.* **125** 1568
[20] Ziegler J F, Biersack J P and Littmark U 1985 *The Stopping and Range of Ions in Solids* (New York: Pergamon)
[21] Netzelmann U 1990 *J. Appl. Phys.* **68** 1800
[22] Dubowik J 1996 *Phys. Rev.* B **54** 1088
[23] Kakazei G N, Kravets A F, Lesnik N A, Pereira de Azevedo M M, Pogorelov Yu G and Sousa J B 1999 *J. Appl. Phys.* **85** 5654
[24] *Numerical Data and Functional Relationships in Science and Technology* 1986 (*Landolt–Börnstein New Series* vol III/19a) (Heidelberg: Springer)
[25] Coey J M D, Douvalis A P, Fitzgerald C B and Venkatesan M 2004 *Appl. Phys. Lett.* **84** 1332
[26] Yamamuro S, Sumiyama K, Kamiyama T and Suzuki K 1999 *J. Appl. Phys.* **86** 5726